Scanning tunneling microscope investigation of carbon nanotubes produced by catalytic decomposition of acetylene

L. P. Biró
KFKI, Research Institute for Materials Science, H-1525 Budapest, P.O. Box 49, Hungary

S. Lazarescu, Ph. Lambin, P. A. Thiry, A. Fonseca, J. B. Nagy, and A. A. Lucas
ISIS, Facultés Universitaires Notre-Dame de la Paix, 61 Rue de Bruxelles, B 5000 Namur, Belgium
(Received 23 December 1996)

A detailed scanning tunneling microscopy (STM) study of carbon nanotubes prepared by catalytic decomposition of acetylene over a supported transition metal catalyst is reported. Nanotubes with diameters in the 10-nm range and others with diameters as small as 1 nm were found. The mechanism of STM image formation and image deconvolution with respect to the tip shape are discussed, as well as the corrections which have to be applied when measuring by STM nanotube diameters in the ranges of 10 nm and of 1 nm, respectively. The behavior of a nanotube crossing steps on the graphite surface is analyzed. Modified height values measured on a single-wall nanotube in regions where it was subjected to strong mechanical stresses indicate changes in the electrical conductivity by several orders of magnitude. Carbon nanotubes are found to be good candidates to be used for STM tip shape characterization in the nm range. [S0163-1829(97)02543-5]

I. INTRODUCTION

Since the first observation of carbon nanotubes[1] and the subsequent report of the conditions for synthesizing large quantities of nanotubes,[2] different methods have been developed to produce and purify macroscopic quantities of this material. A modification of the arc method uses transition metal as a catalyst to enhance the production of single-wall carbon nanotubes.[3] A method based on the catalytic decomposition of carbon containing gas on a transition metal catalyst and subsequent chemical purification resulted in carbon nanotubes with a yield of 23% of C weight.[4,5] More recently, a modification of the vapor growth method[6] using transition metal catalyst has been reported giving a yield of over 70% of single-wall nanotubes (SWNT).[7]

In the past decade, scanning tunneling microscopy[8] (STM) and atomic force microscopy[9] (AFM) became basic tools in the rapidly developing field of nanoscience. An overview of their applications to the investigation of fullerenes and carbon nanotubes has been published recently.[10] The carbon nanotubes which have been investigated by STM can be grouped in two families: The 1-nm diameter range[11–14] and the 10-nm diameter range.[15–18] A number of groups have reported atomic resolution on the outer wall of a nanotube.[12,15,16] It was found that the periodicity of tunneling current maxima is coincident with the value for highly oriented pyrolytic graphite (HOPG), this being an indication that the measured tubes were at least double-wall tubes.

To our knowledge, no detailed STM work has been reported on carbon nanotubes produced by the catalytic decomposition of a gaseous hydrocarbon. In the present paper we report STM investigation of nanotubes produced by catalytic decomposition and we discuss the influence that the tip shape has on the apparent morphology of carbon nanotubes in the STM images, a problem which has received less attention up to now.

II. EXPERIMENT

A. Sample preparation and experimental conditions

The carbon nanotubes were produced by catalytic decomposition of acetylene at 700 °C on a supported Co catalyst, as described earlier.[4,5] Samples were prepared by ultrasonication in toluene of the material resulting from the chemical removal of the catalyst (A type sample); and by ultrasonication in toluene of the material obtained after the chemical oxidation of the A type material in an aqueous solution of $KMnO_4/H_2SO_4$ (B type sample). Both A and B type suspensions were placed on freshly cleaved HOPG and the toluene was evaporated at room temperature.

B. STM results

The samples were examined by STM under ambient conditions, using mechanically prepared Pt tips. Tunneling voltages in the range of 100–400 mV and tunneling currents in the range of 0.2–1 nA were used. The horizontal and vertical calibration of the STM was checked against the HOPG substrate of the samples.

Only tubes with diameters in the 10-nm range have been found in B type samples, with a few exceptions. In A type samples, by contrast, individual tubes and bundles of tubes with 1 nm diameter have been found in addition to the 10-nm diameters. In a single occasion two nanotubes with an estimated diameter in the 1 nm range were found in a B type sample. These nanotubes were partly embedded in amorphous carbon, which made it difficult to determine their exact diameter. The fact that these nanotubes were embedded in amorphous material suggests that they were partially uncovered by the ultrasonication of the sample in toluene, and the amorphous coating may be the reason why they survived the oxidation treatment.

A typical example of tubes of 10-nm diameter, from a B type sample, is shown in Fig. 1. Several nanotubes emerge

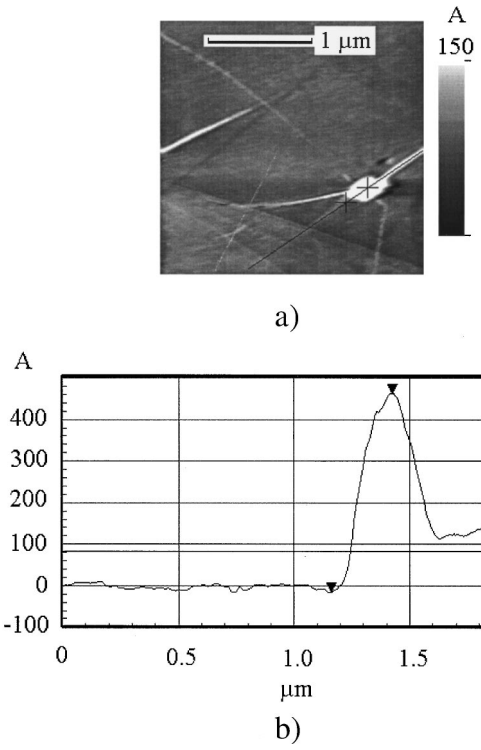

FIG. 1. Constant-current STM image of carbon nanotubes of a 10-nm diameter in a *B* type sample. (a) Plane view image; note the light object (marked with a cross in the center) from which emerge three nanotubes. (b) Line cut along the black line shown in part a; the protruding ''hill'' of 460 Å corresponds to the tip shape; note the plateau in the line cut on the right-hand side of the ''hill'' which corresponds to the height of the nanotube.

from the light object near the lower right corner of the image. The height of the tube along which the line cut is running, is in the 10–12 nm range over a distance of 0.5 μm. We prefer to use the height of the tube for estimating its diameter, for reasons that will be discussed in detail later.

In Fig. 2, a plane view image of a long nanotube is shown from an A type sample. The estimated diameter of the tube is in the 1-nm range. The tube crosses several steps; particularly interesting is the plateau which runs from the lower edge of the image towards the upper right-hand corner. As can be seen from the gray shades, the step height is different on the left- and right-hand sides of the plateau. One can notice from the gray scale given at the right-hand side of the image and from the horizontal image scale, that there is a mismatch between the apparent height and apparent width of the tube. This matter will be discussed in detail later.

Figure 3(a) shows a large scale image of a ''raft'' of parallel nanotubes of 10–20 Å diameters. Figures 3(b) and 3(c) show details taken over the raft. The profile along the line cut marked in Fig. 3(c) is shown in Fig. 3(d). Having a raft of nanotubes with similar diameters is an ideal situation for deconvoluting the tip shape and the tube shape, as will be discussed in more detail later on. In this case one of the parameters which is difficult to determine, namely, the difference in the widths of the tunneling gaps over the support (HOPG in our case) and over the nanotubes, can be discarded. According to the model proposed by Tersoff and Hamann,[19] the tunneling current is dependent on the local

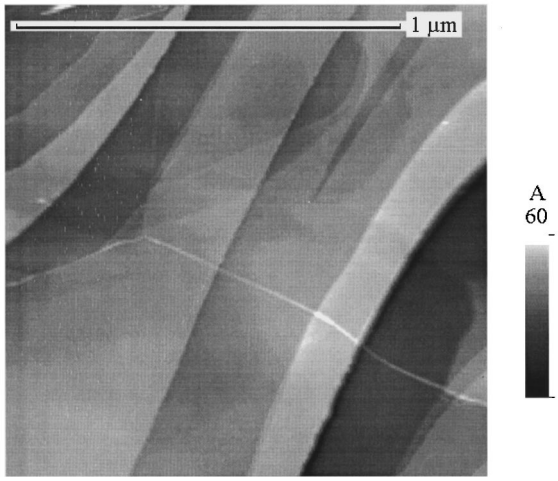

FIG. 2. Constant current plane view image of a single nanotube from an A type sample, crossing a plateau with two unequal steps on both sides. The apparent tube width is in the 160-Å range, while the apparent height of the tube is in the 8–9 Å range. See dimensions in Fig. 4 and Table I.

density of states (LDOS) in the vicinity of the Fermi level, corresponding to the point of the sample surface over which the tip is found. If the nanotubes were lying on a surface made of a different material, such as gold, or had a different electronic structure, the variations of the tunneling current could not be translated into topography in a straightforward way.

The images of nanotubes with diameter in the 1-nm range prepared by the catalytic procedure have been compared with STM images of SWNT ropes prepared by laser ablation as reported in Ref. 7 and used here as size standards. It was found that the nanotubes look similar in the two different samples. This confirms the validity of our estimation of the measured diameter, since the nanotubes prepared by laser ablation are known to have diameter in the 1-nm range.

C. Image analysis and deconvolution

Two diameter ranges of nanotubes (10 and 1 nm) have been observed experimentally. Different aspects of the image formation are to be considered in these two ranges. For instance, in the case of a tube with a diameter of 10 nm one can neglect the effects arising from the different values of LDOS over HOPG and over the tube. It is justified to do so, because the rule of thumb is that a modification by a factor of 10 of the tunneling current induces a variation of the tunneling gap of 1 Å. So, the error produced by the difference in the LDOS is not significant as compared with the total diameter of 100 Å. However the nanostructure of the tip cannot be neglected in this case. It is extremely unlikely to have nanotips with a very high aspect ratio having a length exceeding say 15 nm. This means that the shape of the tip on the last 10 nm will have a significant effect on the apparent topography of the nanotube.

The case of a tube with a diameter of 1 nm is totally different. Here, the variations of the LDOS cannot be neglected. It will be shown that defects in a tube of 1 nm can have a significant influence on the apparent height of the tube on account of the extreme sensitivity of the electrical

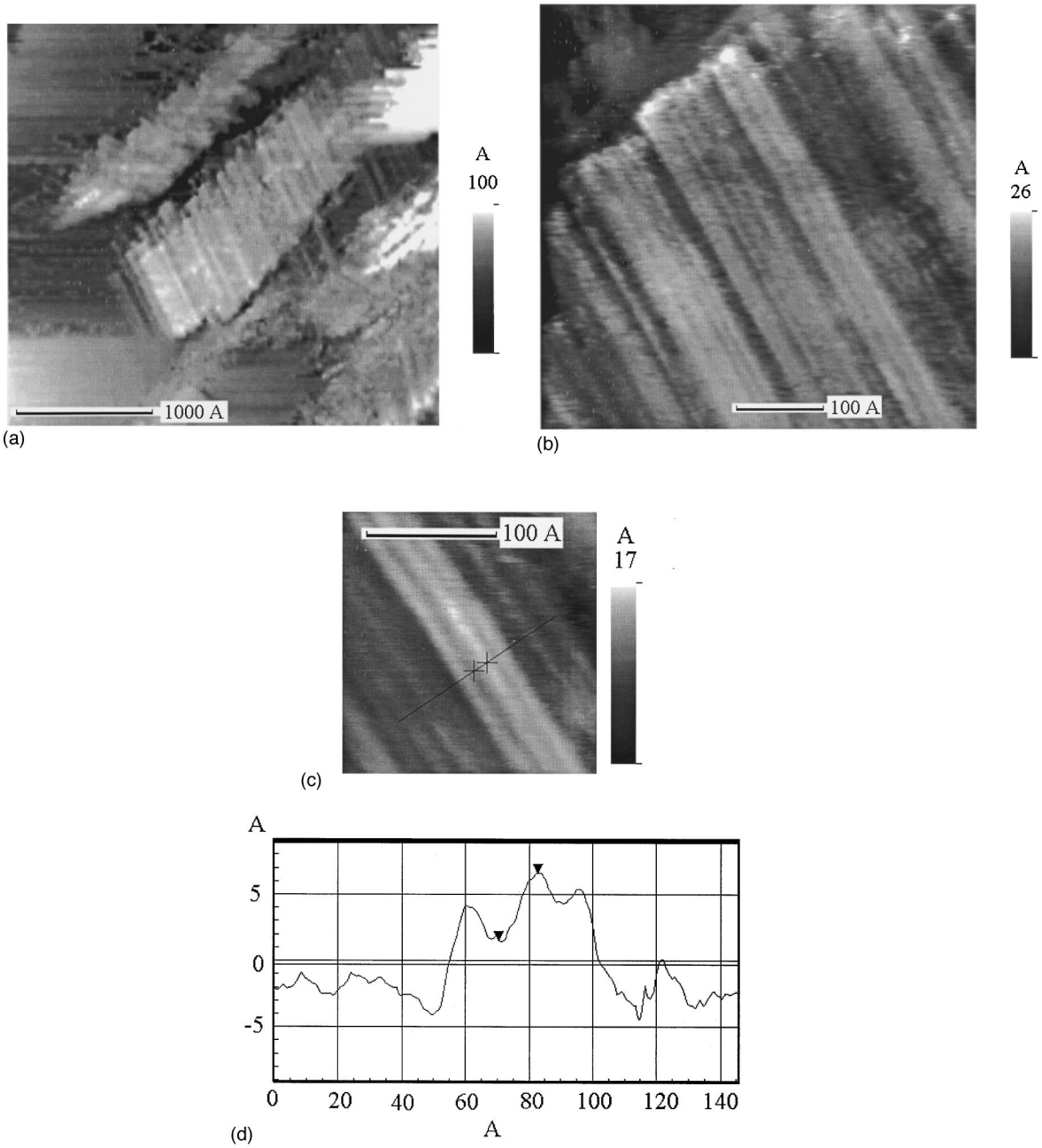

FIG. 3. Constant-current STM images of a bundle of single-wall nanotubes from an A type sample. (a) Large scale plane view image. (b) Detail of part a (image zoomed physically, not by software); note the three nanotubes emerging from the lower right hand corner. (c) Detail of three nanotubes seen in part b emerging from the lower right-hand corner (image zoomed physically, not by software); the line cut along the black line is shown in part d. (d) The line cut marked in part c. See Fig. 7 and Table II for dimensions averaged over five different line cuts.

conductivity of carbon nanotubes to defects.[20] The effect of the nanoshape of the tip can be neglected (the shape on the last 10 nm) if the image is taken with a sharp nanospike. It is possible to have high aspect ratio nanospikes with a length of the order of 15 Å. However, one should not forget that a mechanically prepared tip can have several nanotips of comparable length. This cannot be observed by scanning an atomically flat surface like HOPG, because in this case only the longest nanospike is active. During the scanning of a nanotube however, the cooperative effect of close nanospikes may lead to an apparent increase of the tube height. If the tip is not sharp, its shape can be calculated and taken into account by using the measured profile of steps on HOPG.

1. Nanotubes of 1 nm diameter

In this section the images in Fig. 2, and Fig. 3(c) will be analyzed. The region of the plateau from Fig. 2 is shown schematically in Fig. 4 (region II). The measured apparent dimensions of the tube, i.e., the half diameter $D/2$ and the height h are given in Table I. The numerical values are the result of averaging 10 values from line cuts taken in different

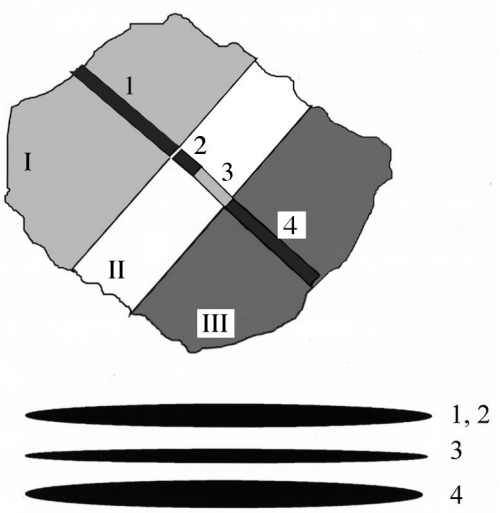

FIG. 4. Model structure of the plateau region seen in Fig. 1. The solid ellipses labeled by numerals show the apparent cross sections built on the basis of the measured dimension given in Table I.

locations in regions 1, 2, 3, and 4. One notices that, while the half diameter values fluctuate within the lateral experimental error, in the vertical direction (which is known to have at least an order of magnitude better resolution than the horizontal direction), there is a clear difference in region 3 as compared with the other regions. The second observation is that the tube seems to have a height only about 20 times smaller than its width. An aspect ratio of that sort is highly unrealistic. In Fig. 4, the cross sections built according to the measured values are shown as black ellipses. The differences in the LDOS of HOPG and of the tube cannot account for this.

One can use the two steps on both sides of the plateau to get information on the tip shape. The height of the step from region I to region II is 10 Å. If one compares the ideal (geometric) step shape with the one measured along a line cut crossing the step, data about the radius of curvature of the tip can be extracted. The topographic profile of the step is extending over 150 Å, which we use as an estimate of the tip half width at the height of 10 Å. The height of the step from region II to region III is 39 Å; here a tip half width of 250 Å is found at 39 Å from the end of the tip. Using these data, and assuming a spherical tip for simplicity, one can calculate a radius of curvature of 975 Å for the tip, i.e., an extremely blunt tip. In Fig. 5(a) a qualitatively similar situation is sketched of a blunt spherical tip imaging a small nanotube. The tip may be regarded as a circle of radius $R+\Delta$, the spherical tip radius plus the width of the tunneling gap, rolling over the circle of radius r representing the nanotube. Several successive positions of the tip are shown in lighter gray. One can notice that the apparent diameter D will exceed several times the real diameter d. The ratio D/d depends on the value of R, r, and Δ. In the range of tunneling currents used here, one can assume that Δ and r are of similar magnitude. With this simplification in mind and using simple geometry, one can estimate r from the formula

$$r=\frac{(D/2)^2}{4R}.$$

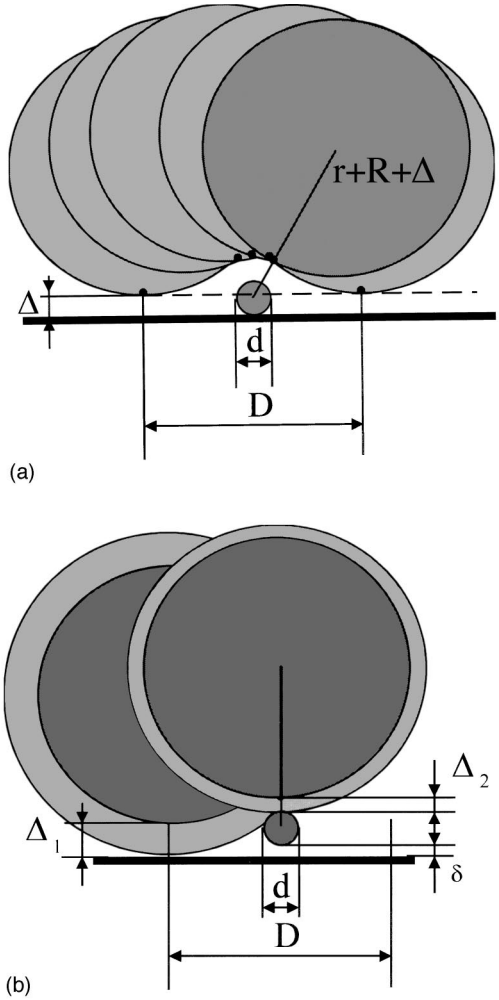

FIG. 5. Convolution effects influencing the apparent diameter of a small nanotube imaged by a blunt tip. (a) Rolling a sphere of radius $R+\Delta$ over a tube of radius r, where Δ is the tunneling gap width, considered identical for HOPG and the nanotube; the small solid dots indicate the point which is considered to be the tunneling point during the image construction. (b) More realistic case where the separation δ between the nanotube and the underlying HOPG and the different tunneling gap widths, Δ_1 for HOPG and Δ_2 for the nanotube, are considered.

Using the values of Table I, a radius of 1.9 Å is estimated for the tube of Fig. 2. This value deviates by a factor of 2–2.5 from the radius values which can be estimated from the height on the undamaged parts of the tube. The deviation shows that the differences in the width of tunneling gap for HOPG and for the nanotube cannot be neglected. If the width of tunneling gap for the nanotube, Δ_2, is smaller than the corresponding value for HOPG, Δ_1, the sphere representing

TABLE I. Measured half diameter, $D/2$, and height, h, in regions 1, 2, 3, and 4 (see Fig. 4) over the nanotube crossing a plateau shown in Fig. 2.

Region	1	2	3	4
$D/2$ (Å)	87±2.88	87±2.65	84±1.72	81±4.64
h (Å)	8.5±0.17	9.2±0.33	5.5±0.21	9.0±0.35

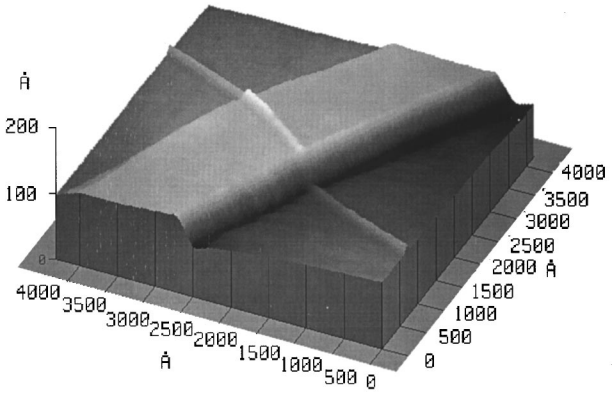

FIG. 6. Three-dimensional detail of the plateau region viewed from the side of 39-Å high step (region III). Note the discontinuity of the tube at the edge of the plateau and the different height values in region II.

the tip will suffer a ''deformation'' while rolling over the nanotube [see Fig. 5(b)] instead of behaving like a rigid body as in Fig. 5(a). When the tip starts rising in the vicinity of the nanotube (due to the additional tunneling current from the nanotube), the distance between the center of the tip and the center of the nanotube becomes $R+\Delta_2+r$, where $\Delta_2<\Delta_1$. As the tube is not an integral part of the underlying HOPG, it is reasonable to expect that under identical conditions, the tunneling current flowing through the tube will be smaller than the tunneling current over the HOPG. This means that in constant-current imaging, the width of the tunneling gap will be reduced over the nanotube as shown in Fig. 5(b). In a situation like that discussed for Fig. 2, one cannot expect a better estimation of the tube radius from the measured D values, unless one finds a reliable way to determine the adsorption distance δ and the difference in tunneling distances $\Delta_1-\Delta_2$. As shown in Fig. 5(b), the opposite contributions of δ and $\Delta_1-\Delta_2$ to the apparent tube height produce the least distortion in the tube dimensions when the tip is right on the top of the nanotube. Therefore, the best value of the diameter is given by the height of the tube.

The measured height values reported in Table I show that the tube crossing the plateau in Fig. 2 is a nanotube with a diameter in the range of 9 Å. This means that it is likely a single-wall nanotube. Coming to the problem of the height measured in region 3, detailed three-dimensional images like that in Fig. 6 reveal that while the tube is continuous from region I to region II, it has broken from region II to region III. Furthermore, the line cuts taken on the tube lying on region II support the idea that the tube has broken in three parts as indicated by gray shades in Fig. 4. It is reasonable to assume that before breaking, the nanotube had to support the highest stresses in region 3 (see the stress calculations below). Therefore, in this region a lot of defects could have been produced. As reported recently, the accumulation of defects can modify the electrical resistivity of a nanotube by several orders of magnitude.[20] So, the apparent height decrease of 3 Å may result from a decrease of the conductivity by three orders of magnitude due to the structural defects accumulated before breaking. If the tube had collapsed into a single graphene layer on the HOPG, a step of 3.35 Å would have been expected together with a simultaneous widening of the structure. It cannot be ruled out that the tube collapsed

TABLE II. Measured half diameter, $D/2$, and height, h, for the three tubes seen in Fig. 3(c).

Tube	1	2	3	Three tubes
$D/2$ (Å)	11.6±1.49	8.6±0.27	13.9±0.70	29.8±0.33
h (Å)	8.0±0.30	10.0±0.24	8.1±0.30	

to amorphous carbon in region 3. However there is no reason to expect that the amorphous carbon deposit will conserve the tube width.

When the tip is sharp enough, one can obtain nearly coincident width and height values. However, in this case too, it is recommended to analyze the images carefully. The deconvolution of the image and that of the line cut shown in Fig. 3(c) and Fig. 3(d), respectively, is simplified by the fact that the three tubes seen in the image lie on top of a bundle of similar tubes as shown in Fig. 3(b). With the assumption that the nanotubes of the bundle were formed under similar conditions (they contain similar numbers of defects), it is reasonable to suppose that the width of the tunneling gap is similar over the tubes of the same bundle. Moreover, the compression effects due to the tunneling tip, if any, should be similar as long as the diameter of the nanotubes does not differ strongly from one tube to the other. With these considerations in mind, one can accept that the measured height values correspond to the real diameter of the tubes. By averaging over different line cuts taken through the image of Fig. 3(c), the values of Table II have been obtained. The different quantities measured are shown schematically in Fig. 7. One can notice from Table II that the sum of the $D/2$ values of the three nanotubes is greater than half the D value of the three-tube unit measured together, which is a geometric impossibility. This result is a consequence of the distorted diameter resulting from the convolution with the tip shape.

Analyzing the data of Table II, and the line cut in Fig. 3(d), one can conclude that the three tubes lie close to each

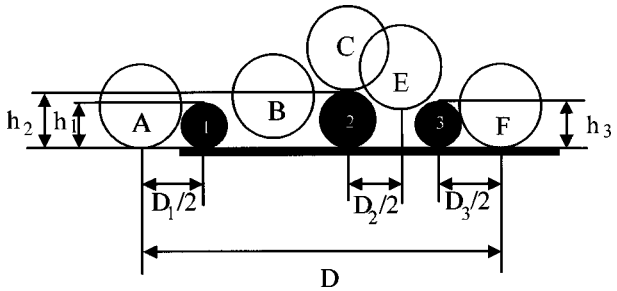

FIG. 7. Schematic representation of the three-tube unit shown in Fig. 3(c). Solid circles numbered 1, 2, and 3 stand for the three tubes, light circles labeled by letters represent the effective tip (tip radius plus tunneling gap width) modeled by a sphere. Different positions during the scan are shown. The quantities which are given as numerical values in Table II are indicated, too. In position A, the tip starts tunneling to tube 1 and starts lifting; in position B, although the separation between tubes 1 and 2 would allow it, the tip does not go down to the base line because of tunneling to both tubes, 1 and 2; in position C, the tip is the tunneling point to the point with tube 2; in position E, the tip tunnels to tubes 2 and 3; in position F, the tip separates from tube 3 and starts tunneling to the base line only.

other but they do not touch. The sum of rounded height values (considered to be closer to the real diameters) is 26 Å, while the total width of the structure is 59.6 ± 0.33 Å. Comparing the h and $D/2$ values for the tubes on the left- and right-hand sides of the group of three tubes, a slightly asymmetric tip shape can be derived, with an average radius of curvature of 14.4 Å. This is an effective value, i.e., the corresponding Δ gap value is included in it. Figure 7 shows the schematic arrangement. The tip starts moving upwards in position A due to the proximity of tube 1. In position B, although the width of the gap between tubes 1 and 2 would allow it, the tip does not go down to the base line, because when it enters between tubes 1 and 2, it starts tunneling to tube 1, to the base line, and to tube 2. So instead of tunneling to a plane, the tip tunnels to a surface which can be modeled by half a cylinder concentric to the tip. In position E, the geometrical width of the gap is smaller than the tip diameter. Therefore, in this case the apparent half width of tube 2 will be smaller than in reality. The 1.3-Å difference between the height and the $D/2$ value of tube 3 in position F, as compared with position A, shows that the tip has a slightly asymmetric shape. To make the analysis simpler, it was supposed that the three nanotubes lie on a flat surface. If one takes into account that they rest on other tubes of similar diameters, the vertical diameter should be 1.13 times the measured height. This yields for the geometrically corrected diameters: 9.0 ± 0.33 Å, 9.1 ± 0.33 Å, and 11.3 ± 0.27 Å, respectively. One can calculate the expected diameters d of the possible nanotubes from the formula,[10]

$$d_t = \sqrt{3} a_{C-C} \sqrt{m^2 + n^2 + mn} / \pi,$$

where $a_{C-C} = 1.421$ Å, m and n being two integers. On that basis and taking in account the stability criterion given in Ref. 7, according to which the armchair (m,m) tubes are the more stable ones, one may tentatively identify the measured tubes as being (7,6) or (7,7), and (9,8), respectively.

2. Nanotubes of 10-nm diameter

As already mentioned, the problems which have to be taken in account in the case of nanotubes of 10 nm in diameter are qualitatively different from those encountered in the case of nanotubes with 1 nm in diameter. The geometry of the tip on a scale of 10 nm is frequently far from being ideal in the case of mechanically prepared tips, which have been widely used for nanotube measurements. A schematic presentation of the problem that may arise is given in Fig. 8. The tip has a sharp spike, and it may be regarded as a very good tip for working on a flat sample. However, if the length of this spike does not exceed the diameter of the nanotube, the image will have important contribution from the flat part of the tip over a significant length of the line cut shown in the figure: regions B, C, and D. As the radius of curvature of the nanotube is smaller than that of the flat region of the tip, over region C, the role of sample and tip will be reversed: the nanotube is imaging the tip. Because of mechanical strength of materials, it is unrealistic to suppose that one can have stable spikes 15-nm long with a diameter of 10 Å, except if one considers using nanotubes themselves for tips, as reported recently by Dai and co-workers.[21] The second problem which should be considered is that cutting a Pt wire

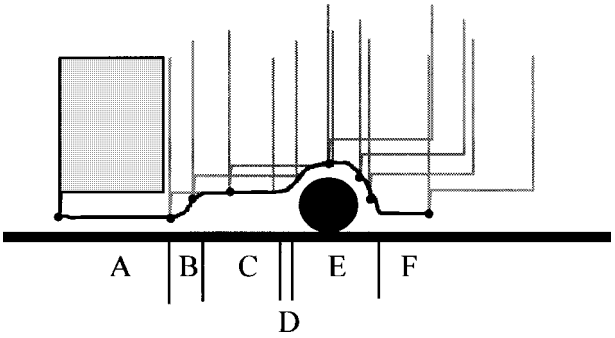

FIG. 8. Schematic representation of a scan line taken by a flat tip with a sharp spike shorter than the diameter of the nanotube, the nanotube is indicated by a solid circle. Several positions of the tip during the scan are indicated by gray lines. The solid line shows the scan line; small solid circles indicate the points which would be used by a hypothetical software for the image construction. Zone A, correct image of the flat surface; zone B, the right-hand corner of the flat region of the tip starts tunneling to the nanotube, however, the points considered for image construction will be those shown by small solid circles; zone B is a transition region; zone C, the nanotube images the flat region of the tip; zone D, transition region; zone E, correct image of the nanotube taken by the sharp spike; zone F, correct image of the flat surface.

yields a huge number of nanotips (spikes). Over an atomically flat surface, the active tip will be the longest one. The situation will be drastically different if the scanned object is a three-dimensional object, since switching from spike to spike will occur while the tip scans the object. So, if the object has a diameter of 10 nm, in most of the cases the resulting image will be a convolution of the sample shape with the averaged tip shape, as seen in Fig. 1(b) in the portion of the line cut which crosses the light object marked in its center by a black cross. The radius of curvature of this object being smaller than the radius of curvature of the tip, it images the tip. It is difficult to establish the nature of this object: it could be an upward pointing nanotube grown together with the three other tubes seen in the image. The stability of the ensemble may be given by the three nanotubes which can be seen in Fig. 1 emerging from the sharp object.

In Fig. 9, two line cuts from consecutive images taken over the nanotube emerging from the sharp object towards the right-hand side of the image in Fig. 1 are shown. As guides for the eyes, the gray ellipses show the cross section of a nanotube of 120 Å in diameter. One can observe that the tube is situated close to a step. The imaging conditions for a flat surface are constant from one image to the other as shown by the same step height of 26 Å in both line cuts. However, the apparent tube shape is different. The shape of the line cut in Fig. 9(b) may be the result of a double tip as shown in Fig. 10. When the main tip is in position B, the point marked by a small solid circle is considered as a tunneling point for the image construction. In fact, the tunneling will take place to another point of the main tip and to the secondary tip, as shown by solid lines. The shape of a line cut through the nanotube marked as a large solid circle is also shown. One may conclude that for the case of nanotubes of 10 nm in diameter, the safest way to measure their diameter is to take a line cut running along the axis of the tube and comparing it to a nearby flat region of the substrate.

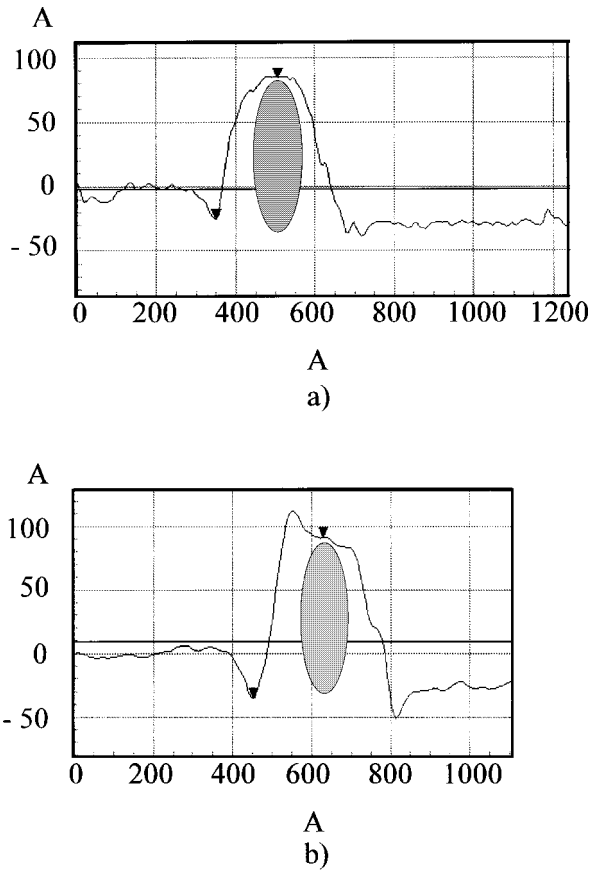

FIG. 9. Two consecutive line cuts taken over the same nanotube shown in Fig. 1, extending to the left hand side of the light object marked in its center by a cross. The gray ellipses are shown to guide the eyes, they correspond to nanotubes with a diameter of 120 Å. Note the constant height difference between the upper side and lower side of the step which runs parallel to the nanotube. The temporary alteration of the shape of the nanotube is due to a secondary tip as shown schematically in Fig. 10(a) without secondary tip; (b) with secondary tip.

III. DISCUSSION

As pointed out in the previous section dedicated to image analysis and deconvolution, several effects have to be considered when using STM to produce images of three-dimensional objects instead of atomically flat surfaces. Unfortunately, frequently in the published papers on carbon nanotubes, very few line cuts were reported and often even the gray scales were omitted from the images. This omission makes an STM image very difficult to interpret. STM has a two orders of magnitude better resolution in the direction perpendicular to the sample surface as compared with the in-plane resolution. As a consequence, most commercially available STM softwares use nonequal axes in image presentation, i.e., the vertical axis is several times extended with respect to the horizontal ones. Therefore, if no gray scale or line cut accompanies the image, it is very hard to decide to what extent the diameter values which are given are accurate. In most of the cases it is not recommended to take the apparent diameter of the nanotube as geometrical diameter, as emphasized above.

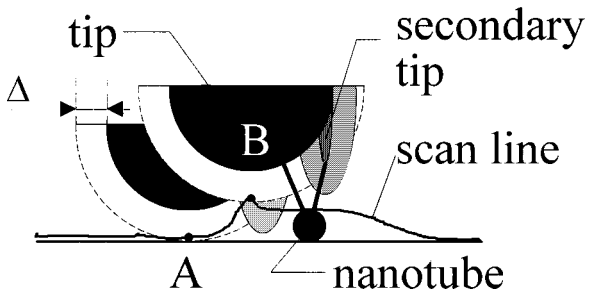

FIG. 10. Schematic representation of the effect on the scan line of a secondary tip developed on the main tip. Compare with experimental line cuts in Figs. 9(a) and 9(b). Small solid circles mark the points considered in image construction, heavy line joining the nanotube and the tips mark the really active tunneling directions.

The presence of nanotubes with both 1-nm and 10-nm diameters in the material resulting from the catalytic process suggests that there are two different mechanisms responsible for the production of nanotubes. The single-wall nanotubes have been reported most frequently when a transition metal catalyst was present during the tube synthesis, irrespective of whether the arc method, laser evaporation, or the catalytic decomposition of carbon containing gas was used. The observation of nanotubes with 1 nm in the material produced by the catalytic method confirms that the factor which enhances the production of single-wall nanotubes is the presence of the transition metal atoms, with less importance played by the physical or chemical status of the material which carries the transition metal. This supports the idea that the transition metal atoms contribute like individual entities to the production process of the single-wall carbon nanotubes. A mechanism which fulfills this criterion is the scooter mechanism proposed by Thess *et al.*[7] The production mechanism of the nanotubes with diameters in 10-nm range seems to be correlated with the size of the catalyst particles. The proposed mechanism is based on the production of C_2 units over the catalyst and their addition to the growing nanotube. As discussed in earlier papers,[22,23] the multiwall nanotubes grow around the catalytic particles. High-resolution transmission electron microscopy supports this mechanism, see Fig. 3(b) in Ref. 23.

The absence of nanotubes with a diameter in the range of 1 nm from most of the B type samples suggests that the single-wall nanotubes were attacked and destroyed during the chemical oxidation of the soot. This can happen very easily if the tube is broken during the previous treatments, or not terminated by a cap. In this case it will be attacked from the open end and will be oxidized. In Fig. 3(b), one notices the same phenomenon as reported by Olk and Heremans[11] that the broken end of the nanotubes is associated with a higher tunneling current. This appears in the image as a brighter end when compared with the body of the tube. This may be the result of dangling bonds. Again, this supports the idea that the single-walled nanotubes with broken ends will be destroyed during the chemical oxidation.

The bending of a nanotube crossing a surface step, as revealed in Fig. 2, was analyzed theoretically by solving the beam equation of elasticity,

$$\frac{d^4z}{dx^4}=\frac{K_z}{EI},$$

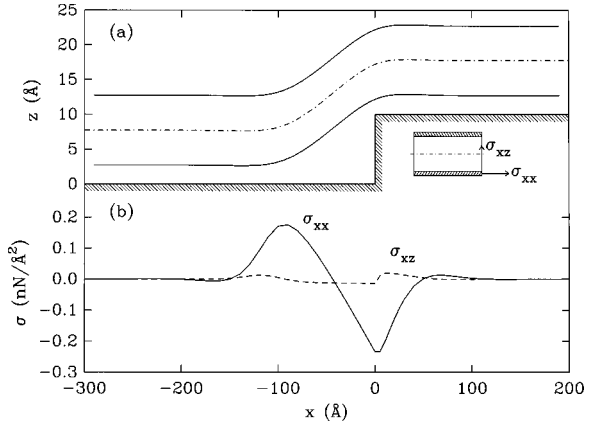

FIG. 11. (a) Bending of a nanotube crossing a 10-Å step on graphite substrate computed from linear elasticity. (b) Longitudinal (full curve) and transverse (dashed curve) stresses along the lowest fiber of the deformed nanotube. The x and z scales in part (a) differ from each other and, so, the apparent tube diameter (10 Å) varies with the slope of its axis.

where $z(x)$ is the curve taken by the axis of the tube when loaded by the force per unit length K_z, E is the Young modulus, and $I=\pi R^3 t$ is the moment of inertia of the beam cross-sectional area, with radius R and an assumed small layer thickness t. The loading force is the one that binds the tube to graphite. It was derived from C-C pair potentials $C_{12}/r^{12}-C_6/r^6$ that were integrated over the semi-infinite substrate and a unit of length of the tube. For a tube with small thickness, K_z is found proportional to t, so the ratio K_z/EI becomes independent of this parameter, and the same holds true for the elastic curve $z(x)$. The potential parameters were taken from Girifalco.[24] With these parameters, the equilibrium distance of a 10-Å diameter nanotube to the continuum edge modeling the graphitic substrate is 2.72 Å. By comparison, a flat carbon sheet would be 2.98 Å above the continuum edge.

Figure 11 shows the results obtained for a nanotube of 10-Å diameter crossing a 10-Å step (three graphite interlayer distances) that aimed at representing the situation realized in Fig. 2 on the smaller-step side of the terrace. In these calculations, the Young modulus of the nanotube had the value recently measured for nanotubes, 1.8 TPa.[25] The graphite substrate was considered as a nondeformable body. The calculations indicate that the deformation of the nanotube is taking place from roughly 200 Å before to 100 Å after the step. These results fit reasonably well the experimental observations. After the step edge, there is a slight overshoot of the nanotube, where it rises above its normal distance from the plateau surface, and reaches its maximum deviation (0.17 Å) 30 Å away from the step.

The stresses computed along the lowest fiber (the generator closest to the substrate) of the nanotube are shown in Fig. 11(b). The transverse stress component σ_{xz}, which was averaged over the cross sectional area of the nanotube, visualizes the interaction with the substrate. The largest interaction is realized just after the step edge, where the nanotube penetrates deeper in the repulsive core of the substrate. The longitudinal fiber stress σ_{xx}, due the curvature of the tube axis, is much larger and it also reaches its maximum amplitude close to the step. As a consequence, the nanotube should be fragile there. The fact that the nanotube in Fig. 2 broke at the edge of the largest step can therefore be understood on these grounds. However, the stresses computed for the tube crossing a 30-Å step were found roughly the same as the ones plotted in Fig. 11 for the 10-Å step. The tube is in some way floating on the repulsive potential from the substrate and it just takes more place to bend when the step height increases.

Considering now the energetics of the problem, the excess of energy ΔE of the deformed nanotube with respect to a broken one whose two halves lie flat on both terraces is composed of two parts: (a) the strain energy, due to the elastic deformation of the nanotube; and (b) the reduction of adsorption energy, which merely concerns that part of the tube that lies over the normal adsorption distance from the lower terrace. If ΔE exceeded the energy of the carbon covalent bonds, the breaking of the nanotube could occur. One can estimate the latter as $4\pi Rt\gamma$, where γ is the surface tension of graphite perpendicular to the basal planes. On the other hand, the excess energy $\Delta E/4\pi Rt$ calculated from the solution of the elastic equation is 0.054 and 0.12 eV/Å^2 for a nanotube crossing a 10- and 30-Å step, respectively. The latter value still is approximately 2 times smaller than γ (0.26 eV/Å 2).[26] It is only with a step about 100-Å high that the energy of a broken nanotube becomes smaller than that of the deformed tube but, still, the breaking of all the C-C covalent bonds at the step would represent a large potential barrier to overcome.

From both the stress calculations and the energetics approach just developed, it can be concluded that the breaking of the nanotube in Fig. 2 was probably caused by the STM tip. The region shown in Fig. 2 was indeed scanned from bottom to top, so that the nanotube was first loaded on the side of the higher step.

IV. CONCLUSIONS

Detailed image analysis and deconvolution has been performed on STM images of carbon nanotubes. This study revealed the existence of 1-nm diameter nanotubes in the samples produced by the catalytic-cracking method. In addition, a number of recommendations stem from the image analysis: (i) if the nanotubes have a diameter in the range of 10 nm and when one can be sure that the nanotubes are lying on a flat surface, the more accurate estimate of their diameter is the measured height value; (ii) if the nanotubes have diameters in the range of 1 nm, due to the different LDOS over the support and over the nanotube, the use of support materials other than graphite may complicate the image formation beyond a desirable level; (iii) in the case of nanotubes with a diameter of 1 nm the most advantageous situation is when one can choose a flat lying bundle and try to determine the dimensions of the tubes in the topmost layer; however, even in this case, the geometry of the system has to be analyzed carefully; (iv) even blunt tips may be used to estimate diameters of the order of 1 nm if one can be sure that the nanotube is lying on a flat surface and other structures, like steps on the HOPG surface, are used to characterize the tip shape.

The variation of the apparent height of the nanotube crossing the step in Fig. 2 shows that due to accumulation of defects when subjected to high levels of mechanical stress,

the electrical properties of a carbon nanotube may suffer a strong modification.

The simultaneous presence of tubes with 1-nm diameter, and tubes with 10-nm diameter suggests that there are two different formation mechanisms during the nanotube production by catalytic decomposition of a gaseous hydrocarbon over a transition metal catalyst.

The fact that in the *B* type sample only nanotubes with the diameter in the 10-nm range have been found is an indication that the oxidation treatment destroys the single-wall nanotubes.

Due to their cylindric shape, carbon nanotubes are good candidates for being used to characterize the shape of the STM tip in the nm range. Nanotubes may play a similar role for STM and AFM as the latex or gold spheres have in scanning electron microscopy.

ACKNOWLEDGMENTS

The authors wish to thank to Dr. D. T. Colbert for providing samples of single-wall nanotubes and to D. Bernaerts for helpful discussions. L. P. Biró gratefully acknowledges the financial support of CGRI of the French Community of Belgium and of the Facultés Universitaires Notre-Dame de la Paix, Namur, Belgium. This work has been partly funded by the Interuniversity Research Program on Interfacial Materials and Mesoscopic Structures initiated by the Belgian Science Policy Programming (PAI-IUAP P3-49). The work in Hungary was supported by AKP Grant No. 96/2-637.

[1] S. Ijima, Nature (London) **354**, 56 (1991).
[2] T. W. Ebbesen and P. M. Ajajan, Nature (London) **358**, 320 (1992).
[3] D. S. Bethume, C. H. Kiang, M. S. deVries, G. Gorman, R. Savoy, J. Vasquez, and R. Beyers, Nature (London) **363**, 605 (1993).
[4] V. Ivanov, J. B. Nagy, Ph. Lambin, A. Lucas, X. B. Zhang, X. F. Zhang, D. Bernaerts, G. Van Tendeloo, S. Amellinckx, and J. Van Ladyst, Chem. Phys. Lett. **223**, 329 (1994).
[5] A. Fonseca, K. Hernadi, J. B. Nagy, D. Bernaerts, and A. A. Lucas, J. Molec. Catal. **107**, 159 (1996).
[6] T. Guo, P. Nikolaev, A. Tess, D. T. Colbert, and R. Smalley, Chem. Phys. Lett. **215**, 49 (1995).
[7] A. Thess, R. Lee, P. Nikolaev, H. Dai, P. Petit, J. Robert, C. Xu, Y. H. Lee, S. G. Kim, A. G. Rinzler, D. T. Colbert, G. E. Scuseria, D. Tománek, J. E. Fischer, and R. E. Smalley, Science **273**, 483 (1996).
[8] G. Bining, H. Rohrer, Ch. Gerber, and E. Weibel, Phys. Rev. Lett. **49**, 57 (1982).
[9] G. Bining, C. F. Quate, and Ch. Gerber, Phys. Rev. Lett. **56**, 930 (1986).
[10] M. S. Dresselhaus, G. Dresselhaus, and P. C. Eklund, *Science of Fullerenes and Carbon Nanotubes* (Academic Press, San Diego, 1996).
[11] C. H. Olk and J. P. Heremans, J. Mater. Res. **9**, 259 (1994).
[12] M. Ge and K. Sattler, Science **260**, 515 (1993).
[13] M. Ge and K. Sattler, J. Phys. Chem. Solids **54**, 1871 (1993).
[14] K. Sattler, Carbon **33**, 915 (1995).
[15] S. Xie, N. Li, Z. Zhang, W. Lu, G. Wang, S. Qian, and C. Fu, J. Mater. Sci. **30**, 2291 (1995).
[16] N. Lin, J. Ding, S. Yang, and N. Cue, Carbon **34**, 1295 (1996).
[17] Z. Zang and C. M. Lieber, Appl. Phys. Lett. **62**, 2792 (1993).
[18] W. Rivera, J. M. Perez, R. S. Ruoff, D. C. Lorents, R. Malhotra, S. Lim, Y. G. Rho, E. G. Jacobs, and R. F. Pinizotto, J. Vac. Sci. Technol. B **13**, 327 (1995).
[19] J. Tersoff and D. R. Hamann, Phys. Rev. Lett. **50**, 1998 (1983).
[20] T. W. Ebbesen, H. J. Lezec, H. Hiura, J. W. Bennett, H. F. Ghaemi, and T. Tio, Nature (London) **382**, 54 (1996).
[21] H. Dai, J. H. Hafner, A. G. Rinzler, D. T. Colbert, and R. E. Smalley, Nature (London) **384**, 147 (1996).
[22] A. Fonseca, K. Hernadi, J. B. Nagy, Ph. Lambin, and A. A. Lucas, Synth. Met. **77**, 235 (1996).
[23] K. Hernadi, A. Fonseca, J. B. Nagy, D. Bernaerts, A. Fudala, and A. A. Lucas, Zeolites **17**, 416 (1996).
[24] L. A. Girifalco, J. Phys. Chem. **96**, 858 (1992).
[25] M. M. J. Treacy, T. W. Ebbesen, and J. M. Gibson, Nature (London) **381**, 678 (1996).
[26] M. S. Dresselhaus, G. Dresselhaus, K. Sugihara, I. L. Spain, and H. A. Goldberg, *Graphite Fibers and Filaments* (Springer-Verlag, Berlin, 1988), p. 147.